Sancho-Fornes, G.; Avella-Oliver, M.; Carrascosa Rubio, J.; Puchades, R.; Maquieira Catala, A. (2021). Interferometric multilayered nanomaterials for imaging unlabeled biorecognition events. Sensors and Actuators B Chemical. 331:1-9. https://doi.org/10.1016/j.snb.2020.129289

Interferometric multilayered nanomaterials for imaging unlabeled biorecognition events

Gabriel Sancho-Fornes[a], Miquel Avella-Oliver[a,b,*], Javier Carrascosa[a], Rosa Puchades[a,b], Ángel Maquieira[a,b,*]

[a] Instituto Interuniversitario de Investigación de Reconocimiento Molecular y Desarrollo Tecnológico (IDM), Universitat Politècnica de València, Universitat de València, Camino de Vera s/n, 46022 Valencia, Spain.

[b] Departamento de Química, Universitat Politècnica de València, Camino de Vera s/n 46022, Valencia, Spain.

*Corresponding author.

E-mail addresses: miavol@upv.es (M. Avella-Oliver), amaquieira@qim.upv.es (A. Maquieira).

Abstract

There is an intense scientific activity on nanomaterials for biosensing, supported by their great potential to conceive powerful applications in chemistry, biology, and medicine. In addition to meet the required analytical parameters, the social impact of these advances is also highly influenced by cost, simplicity, and portability aspects, which are critical in label-free systems. This paper addresses the design, development, and experimental assessment of multilayered nanomaterials to transduce unlabeled biorecognition assays as both constructive and destructive interferences, by means of simple and effective imaging setups. The materials rely on superposed nanometric films of metals (gold and Ag-In-Sb-Te alloy) and a dielectric (zinc sulphide) deposited on a polymeric substrate. They are tailored to display maximal (constructive and destructive) interferences for immunoassays performed on their surface, and then fabricated by sputtering and characterized by focused ion beam scanning electron microscopy. Herein we also address the development of a simple optical setup that exploits standard DVD laser units to scan by imaging the reflected interferometric response of microarrayed immunoassays. The bioanalytical performance of the approach is experimentally assessed using a representative model immunoassay (BSA/anti-BSA) and a competitive immunoassay to quantify a low molecular weight drug (sulfasalazine), reaching detection limits of 460 and 11 ng mL^{-1} of unlabeled targets, respectively. This study also explores

two alternative one-shot interferometric imaging approaches that provide insights into simpler and faster strategies for label-free biosensing.

Keywords: Interferometry, nanomaterial, imaging, biosensor, label-free, sulfasalazine.

1. Introduction

There is a demand for new materials and bioanalytical schemes that pave the way towards simpler and faster analytical systems and support the dissemination of biosensors across communities [1,2]. Among many other scenarios, it projects a great impact in clinical diagnosis, where these systems strongly favor fast decision-making in emergency medicine and early treatment of acute diseases [3]. A key role in this issue is played by the biosensing advances that point towards the ASSURED criteria (Affordable, Sensitive, Specific, User-friendly, Rapid and robust, Equipment-free, and Deliverable to end users) outlined by the World Health Organization [4]. Therefore, a central aspect to support the potential impact of biosensing out of specialized labs relies on simplicity, cost effectiveness, and portability of the bioanalytical developments.

Along these lines, interferometry is an important transduction principle exploited in the state-of-the-art to sense biomolecular interactions [5,6]. The interferometric approaches for biosensing are typically based on materials tailored to guide light through different paths and measure the interference introduced by the resulting thickness of a biorecognition assay, performed on one of the paths. Some paradigmatic examples are Mach-Zehnder [7], Young [8], and dual polarization interferometry [9], which have proven great biosensing capabilities, whereas they tend to involve rather high nanofabrication requirements per assay, which often affects the simplicity and multiplexing capabilities of the resulting bioanalytical systems.

An interesting alternative are the nanostructures for common-path interferometry [10], such as arrayed imaging reflectometry [11], reflectometric interference spectroscopy [12], and interferometric reflectance imaging sensing [13]. Instead of splitting the light into reference and assay paths, these materials induce an interference of a single beam with itself, to be typically measured by reflectance. As a result, these approaches tend to be less complex and present a higher scalability and multiplexing capabilities.

Herein we address the development of common-path interferometric nanomaterials to analyze multiplexed biorecognition assays in a simple and effective reflectance-based measurement system. The hypothesis behind this idea relies on multilayered nanometric films designed to generate a phase difference in the reflected beams and tailored to be especially sensitive to additional phase differences introduced by nanometric layers of biological matter on their surface. This approach aims to quantify biorecognition assays as intensity changes in the reflected light, generated by the interferences associated to the evolution of the biolayer thickness along the assay (Fig. 1A).

In this work, we investigate multilayered interferometric nanomaterials based on nanometric films of metals (gold and Ag-In-Sb-Te alloy) and a dielectric (zinc sulphide), as optically-active layers to modulate the interference of an incident beam for biosensing purposes. Insights into this direction were studied by Gopinath et al. by sensing the intensity cross sections of assays developed on compact disks [14,15]. This study introduces a new approach to perform multiplexed label-free assays on large-scale interferometric materials, fabricated by industrially-available technologies, and quantified by imaging using simple and unexpensive detection setups.

Herein we report the design, development, and bioanalytical assessment of multilayered nanomaterials aimed to generate great destructive and constructive interferences as response of biorecognition assays microarrayed on their surface. The work firstly explores, by theoretical calculations, the optical behavior of a range of multilayered profiles in biorecognition conditions. From these results, two configurations (constructive and destructive) were fabricated by sputtering on polycarbonate plates and characterized by electron microscopy. This study also investigates simple optical setups to measure the reflected interferometric response of these label-free microarrayed assays by imaging. Along these lines, the development of a laser-scanning setup based on standard DVD laser units is reported, and insights into alternative one-shot interferometric imaging systems are provided and discussed. The bioanalytical performance of this approach is experimentally assessed by means of a representative model immunoassay (BSA/anti-BSA) and a competitive immunoassay to quantify low molecular weight organic compounds, both label-free.

2. Materials and methods

2.1 Chemicals

Carbonate buffer (50 mM sodium carbonate, pH 9.6), PBS-T (8 mM Na_2HPO_4, 2 mM KH_2PO_4, 137 mM NaCl, 2.7 mM KCl, 0.05 % (v/v) Tween-20, pH 7.4), and washing

solutions were prepared with purified water (Milli-Q, Millipore Iberica, Madrid, Spain) and filtered through 0.22 µm polyethersulfone membranes (Merck, Darmstadt, Germany). Bovine serum albumin (BSA), anti-BSA polyclonal IgGs produced in rabbit, sulfasalazine, and ovalbumin (OVA) were supplied by Sigma-Aldrich (Madrid, Spain). Protein-hapten conjugates (OVA-S8) and rabbit polyclonal antiserum for sulfasalazine (anti-sulfasalazine) were produced as described elsewhere [16]. The sputtering targets of zinc sulphide (ZnS) and Ag-In-Sb-Te alloy were from Able Target Limited (Nanjing, China).

2.2 Nanomaterials

The interferometric materials were constituted by stacked nanometric films of gold, zinc sulfide, and an Ag-In-Sb-Te alloy on polycarbonate chips. The thickness of each film was optimized through theoretical calculations performed with the Reflectance Calculator (Filmetrics inc., San Diego, CA, USA), considering a refractive index of 1.47 for proteins. To fabricate the nanomaterials, flat polycarbonate plates (600 µm of thickness) were cut into squared chips (1.5 x 1.2 cm) using a drilling machine (CCD, Bungard, Karo, Germany). All the layers were then coated on the chips, one by one, using an ultra-high vacuum magnetron sputterer (ATC series, AJA International Inc., North Scituate, MA, USA). The thickness and refractive index of the deposited films were determined along the fabrication process by X-Ray reflectivity/diffractometry (X'pert Pro, PANalytical, Almelo, The Netherlands) and spectroscopic ellipsometry (GES5, Semilab, Budapest, Hungary), respectively.

The resulting multilayered structures were characterized by focused ion beam coupled to field-emission scanning electronic microscopy (FIB-FESEM). For that, the nanomaterials were coated by platinum to improve the quality of the scans, micrometric trenches were dug on them using a focused beam of Ga^+, and the thickness profiles were scanned by FESEM (54º tilt).

2.3 Optical setups

Two custom optical setups were developed to measure by imaging the interferometric response of multiplexed biorecognition assays on the nanomerials: a laser-scanning system to perform quantitative measurements (section 3.2 and 3.3) and a one-shot RGB detection system to provide insights into alternative perspectives (section 3.4).

The first setup exploits the laser units of standard DVD drives. They are inexpensive and compact devices that integrate an arrangement of optical elements highly suitable to carry out the reflectance interferometric events generated by biorecognition assays on

these materials. As shown in Fig. 1B, these laser units incorporate a beam splitter that directs a linearly polarized beam (λ = 650 nm) towards the nanomaterial through a λ/4 wave plate that changes the polarization into circular. Then, the laser is reflected back by the nanomaterial and the circular polarization of the beam becomes inverted. Finally, the λ/4 wave plate induces a linear polarization that is perpendicular to the first one, and the reflected beam transmits through the beam splitter towards a photodiode.

To arrange this detection setup, a DVD laser unit (LPC-819R, LG Electronics Inc., Englewoods Cliffs, USA) was set to orthogonally irradiate the nanomaterial, and a planar silicon photodiode (SLC-61N2, Silonex Inc., Montreal, Canada) was positioned to collect the intensity of the reflected beam (Fig. 1B and Fig. S1A). A data acquisition board (DAQ USB-2527, Measurement Computing, Norton, MA, USA) was connected to the optical setup and to a personal computer, to monitor the signal from the photodiode and to stabilize the laser intensity [17].

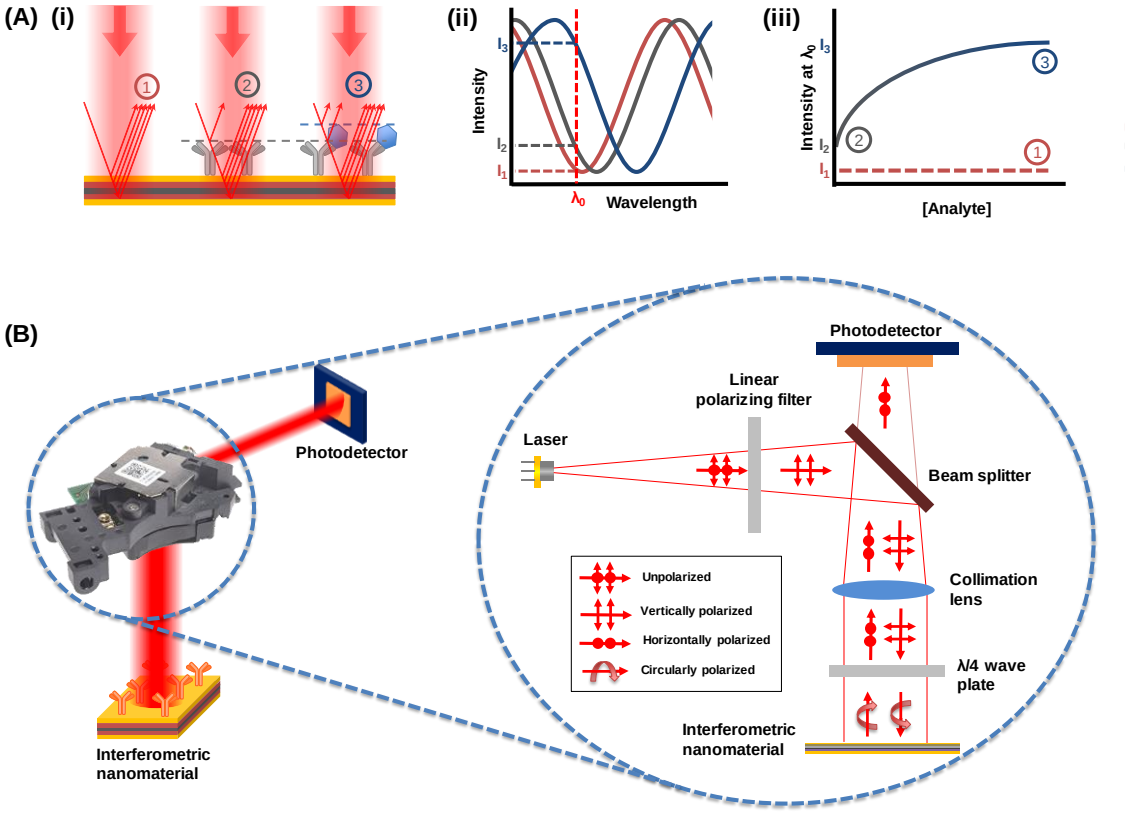

Fig. 1. General scheme of the detection strategy. (A) Illustration of (i) the interferometric sensing principle, (ii) the spectral response along the different stages of an immunoassay, and (iii) the corresponding dose-response curve. (B) Scheme of the laser-scanning optical setup used in this work to perform quantitative imaging measurements of immunoassays carried out on the interferometric materials.

To scan the interferometric response along the nanomaterials, a custom automatized positioning stage was used to hold and sequentially move them under the laser unit (Fig. S1A). This stage is based on two sled motors from standard DVD drives (one for each direction) controlled by an Arduino Uno microcontroller (Arduino, Turin, Italy). The reflected intensities acquired before the assay were subtracted to the ones after it, as an experimental flattening strategy. Finally, the data were arranged as XYZ matrixes and represented as images (using Origin Pro 8, OriginLab Corporation, Northampton, USA) that display the interferometric response of the microarrayed biorecognition assays on the surface of the nanomaterials.

On the other hand, the one-shot RGB imaging system was based on a lateral diffuse irradiation from a regular white LED bulb and a handheld digital microscope (Dino-Lite AM413MZT, AnMo Electronics Corp., New Taipei City, Taiwan) set on the nanomaterial (Fig. S1B). The resulting microarray images were flattened using a polynomial subtraction (using Gwyddion) [18], and denoised with a low-pass Fourier filter as described elsewhere [19]. Finally, the RGB channels of these images were obtained by Photoshop (Adobe, San Jose, CA, USA), and the reflected intensities of the microarrayed immunoassays were quantified in the red channel using the software Genepix (Axon Instruments, Union City, CA, USA).

2.4 Biorecognition assays

Two assays were set up in this study by means of probe microarrays printed on the surface of the nanomaterials: a model immunoassay based on BSA as probe and anti-BSA IgGs as target, and a competitive immunoassay to determine the drug sulfasalazine.

For the first assay, BSA solutions (100 µg/mL in carbonate buffer) were arrayed (40 nL/spot) on the surface of the materials using a noncontact printer (AD 1500, Bio-Dot Inc., Irvine, CA, USA) under controlled temperature (25ºC) and relative humidity (95%), and incubated overnight at 4 ºC to immobilize these protein probes by physisorption. Afterwards, the nanomaterials were washed with PBS-T, rinsed with deionized water, and dried by air stream. To perform the selective IgG biorecognition, anti-BSA solutions in PBS-T (1 µL/spot) were incubated (20 min, room temperature) in concentrations ranging from 1 mg/mL to 10 ng/mL by serial dilutions of $1/10^{0.5}$, including 0 ng/mL. Finally, the nanomaterials were rinsed and dried as before.

For the sulfasalazine immunoassay, OVA-S8 solutions (200 µg/mL in carbonate buffer) were arrayed, incubated on the surface of the nanomaterials, rinsed, and dried as described above. Then, to perform the dose-response curves in this competitive assay, a constant concentration of anti-sulfasalazine IgGs in PBS-T (100 µg/mL) were mixed with different concentrations of sulfasalazine ranging from 100 µg/mL to 3.2 ng/mL by serial dilutions of $1/10^{0.5}$ (including 0 ng/mL). Right after mixing, these solutions were dispensed onto the microarrays (1 µL per spot) and incubated for 20 min at room temperature. Finally, the surfaces were rinsed with PBS-T and deionized water, and dried under air stream.

2.5 Data processing

After both immunoassays, the microarrays on the nanomaterials were analyzed with the measurement setups described above. The analytical signal was the intensity variation of the reflected light before and after each assay. Experimental noise values were calculated as the standard deviation from ten blank measurements (without target), and signal-to-noise ratios (SNR) were obtained by dividing the analytical signals by this noise. The limits of detection and quantification were inferred as the experimental concentration corresponding to the signal of the blank plus three or ten times the SNR values, respectively. To calculate the SNRs, the sign of the analytical signal was inverted in those configurations where the intensity of the reflected signal decreases when the analyte concentration increases (BSA/anti-BSA system on destructive materials and sulfasalazine immunoassay on the constructive ones).

3. Results and discussion

3.1 Interferometric nanomaterials

This study addresses the development of interferometric multilayered nanomaterials to quantify microarrayed biorecognition assays by simple imaging setups. For that, the multilayered structures must be tailored to generate a suitable interferometric response by which nanometric changes in the thickness of biological layers, generated by binding events on the material, display great reflectance changes (Fig. 1A). This section tackles the design of these structures through theoretical simulations, their fabrication, and the characterization of the resulting multilayers.

The top layer of the nanomaterials consists of a thin (5 nm) coating of gold on which to perform the biorecognition assays. This metal was selected for its beneficial features of ease in sputtering and biomolecular immobilization [20]. Moreover, this 5 nm thick layer

of gold is highly transparent and allows almost 90 % of the incident light to transmit through the underlying structure. Below this initial coating, the nanomaterial comprises a film of Ag-In-Sb-Te alloy sandwiched between two layers of ZnS. Given the high refractive index contrast of these materials ($RI_{Ag\text{-}In\text{-}Sb\text{-}Te} \approx 4.0$ and $RI_{ZnS} \approx 2.3$, Table S1), this three-layered structure generates great multilayer reflections, which are mainly responsible for the interferometric properties of the nanomaterial. This particular sandwiched structure was also selected because it is employed as data recording material in standard rewritable compact disks [21,22], so the ASSURED potential of the resulting interferometric biosensors is strongly supported by the already existing technologies to fabricate this multilayer in an inexpensive and large-scale fashion. Successively, the nanomaterial comprises a 50 nm gold film to act as a mirror and reflect the light back to the multilayer, thus enhancing the interferometric response and favoring its measurement by reflectance. Finally, flat polycarbonate plates were employed as substrates on to build this multilayered material. This polymer is easy to handle, presents a good adhesion for sputtered gold, and the bioanalytical developments on polycarbonate involve appealing lab-on-a-disk perspectives for labelled and label-free biosensing [23–25].

The optical behavior of these materials was explored to transduce biorecognition events by means of both constructive and destructive interferences. For that, firstly the interferometric response of different multilayer configurations was assessed by calculating the reflectance variation of a red (650 nm) beam for a thickness change of a biorecognition assay on the material from 0 to 20 nm. In short, these calculations are based on the complex-matrix form of the Fresnel equations and provide the reflected intensity at a given wavelength considering the thickness and refractive index of each layer [26]. The calculations consist of a bi-parametrical screening of the thicknesses of both ZnS films (upper and lower) for a range of thicknesses of Ag-In-Sb-Te alloy (one plot for each alloy thickness). Negative values in these graphs indicate destructive interferences introduced by the assay, positive values mean constructive interferences, and larger absolute values indicate in both cases greater signal changes and potentially higher bioanalytical sensitivity.

As shown in Fig. 2 and Fig. S2, the interferometric response along the variation of the thickness of both ZnS films displays a common trend defined by three main areas. The first one is a rather insensitive area at low thicknesses values, where biorecognition assays generate neglectable interferences (blue region). Then, when the thicknesses increase, the biological layer introduces a long valley of destructive interference (purple strip) that reaches an intensity reduction in the reflected light of up to a 4 %. Next, further

thickness increments in both ZnS layers display a steep ridge of constructive interference of up to a positive 6% (reddish region). Furthermore, when comparing all the plots, it can be observed that these three main areas progressively move towards thinner values of ZnS films when the thickness of Ag-In-Sb-Te alloy increases.

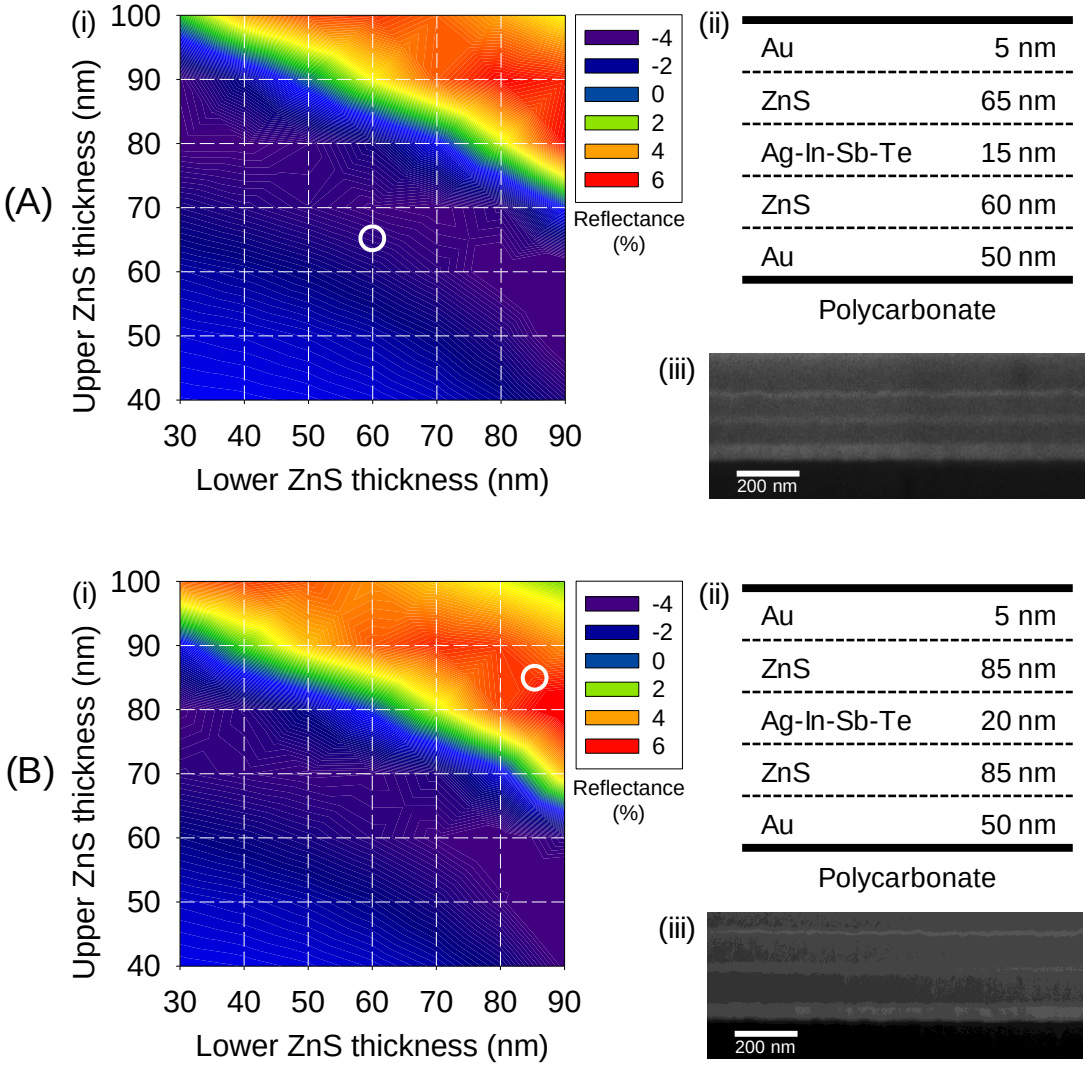

Fig. 2. Design and characterization of the multilayered nanomaterials. (i) Bi-parametric simulated assessment of the interferometric response displayed by a change in the thickness of the biological layer on the material from 0 to 20 nm, at different thicknesses of both ZnS films, and for Ag-In-Sb-Te thicknesses of (A) 15 nm and (B) 20 nm. Color legends indicate the changes in the reflected intensity in percentage (considering the intensity of the incident beam as 100%). See Fig. S2 for the plots at additional Ag-In-Sb-Te thicknesses. (ii) Scheme of the selected multilayered structure for the (A) destructive and (B) constructive interferometric nanomaterials. (iii) FIB-FESEM images of the (A) destructive and (B) constructive multilayers. From bottom to top, the first black layer is the polycarbonate substrate, the whitish film on it corresponds to gold, and the following greyish-whitish-greyish layers correspond to the Ag-In-Sb-Te alloy sandwiched

between ZnS. The upper whitish film is the 5 nm gold coating, and the top greyish layer is a platinum coating deposited to improve the quality of the scans.

As observed, similar interferometric responses are displayed by different thickness profiles. From these results, we selected the configuration schematized in the Fig. 2A (ii) to create the destructive interferometric nanomaterials and the configuration in Fig. 2B (ii) for the constructive one. These structures involve a deep destructive valley and a high constructive ridge (respectively), they keep a balanced distribution of thicknesses along the different layers, and they comprise two different configurations to be experimentally investigated. The reflected intensity of these two structures along a range of thicknesses of biological layer was also simulated, and the results show a well-correlated ($R^2 > 0.999$) linear trend in both cases (Fig. S3).

The selected configurations were fabricated by depositing one by one all the films by sputtering, and the resulting nanomaterials present a good adhesion between layers. To characterize the fabricated materials, micrometric ditches were created on them by FIB and the thicknesses profiles were analyzed by FESEM. As shown in Fig. 2, both multilayered structures are revealed in the microscopy images and all the films are homogeneously distributed, as expected.

3.2 Measurement system

This section addresses the development of a laser-scanning imaging system to measure the interferometric response of microarrayed biorecognition assays on the nanomaterials. In addition to ensuring that the required bioanalytical parameters are met in the resulting assays, this detection setup also aims to provide insights into simplicity, low cost, and portability of the system in order to support the scope of the resulting biosensor. Along these lines, herein we conceive a monochromatic (650 nm) imaging interferometric system that fully exploits the standard laser units of DVD drives. These are inexpensive (about 12 €), robust, and compact (4 x 3 x 1.5 cm) devices that integrate all the elements to be adapted for scanning the interferometric reflectance changes generated by biorecognition assays on the nanomaterials (Fig. 1B). The laser units also comprise a photodiode that monitors the laser intensity, used in this development to successfully keep a constant laser intensity along the measurements by implementing an automatic laser power control algorithm (Fig. S5).

To scan the microarrayed assays, the nanomaterials were placed on a custom positioning system that automatically moves them under the perpendicular irradiation of the laser unit (Fig. S1A). Then, the reflected laser intensities are acquired along the scanning process and rearranged (considering the motion of the positioning system) to

build an image. As shown in Fig. 3, this imaging strategy enables to obtain the bi-dimensional interferometric profiles of microimmunoassays on the nanomaterials. These results constitute the first proof in this work towards empirical biosensing, and they also demonstrate that both multilayers experimentally present the destructive and constructive profiles for which they were designed.

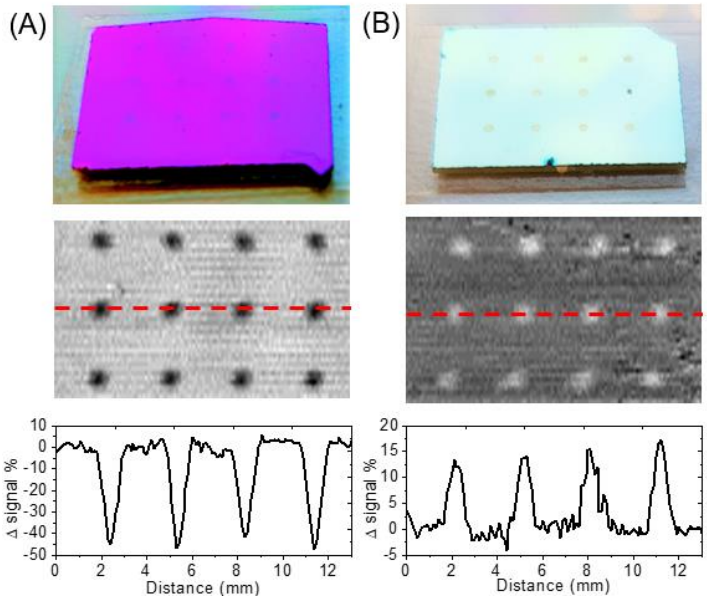

Fig. 3. Photographs (top), resulting interferometric images measured with the laser-scanning setup (middle), and their corresponding intensity cross-section profiles along the dashed red lines (bottom) for the (A) destructive and (B) constructive interferometric nanomaterials. The microarrays consist of immobilized OVA-S8 dots after the incubation of specific anti-sulfasalazine IgGs (100 µg/mL). Normalized signals are represented in the cross-section profiles, where 0 % corresponds to the reflected intensity without biological layer.

3.3 Immunosensing

To assess the bioanalytical performance of the approach in experimental biorecognition conditions, microarrayed immunoassays were performed on the surface of the destructive and constructive nanomaterials and measured with the laser-scanning system described above. Firstly, an immunoassay based on BSA probes to quantify selective anti-BSA IgG targets in solution, was carried out. This immunological system is commonly used for proof-of-concept purposes [27], whereas BSA also has an important role in many biological functions [17]. For example, this protein is responsible for most of the allergic reactions to cow milk and beef, and it could be also involved in the autoimmune response leading to diabetes mellitus [28,29].

As shown in Fig. 4A, well-correlated dose-response curves were obtained for the BSA/antiBSA model immunoassay measured by both constructive and destructive

interferences in label-free conditions. The constructive nanomaterial displayed lower SNR values, and it achieved detection and quantification limits of 3.12 and 5.77 µg mL^{-1} of IgG, respectively. On the other hand, the destructive multilayer presented greater signal variations and a lower noise ($noise_{destruc.}$ = 0.08 a.u. and $noise_{construc.}$ = 0.16 a.u.). As a result, the sensitivity with this multilayer becomes about one order of magnitude higher and reaches detection and quantification limits of 0.46 and 1.49 µg mL^{-1} of unlabeled IgG, respectively. Those are promising sensitivities, obtained with the simple laser-scanning setup herein developed, and fall within the range of other novel label-free developments in the state-of-the-art of optical biosensing as shown in Table 1, including demonstrations performed with the same bioreagents and measurements carried out with commercial detection systems. In addition, this is a suitable and useful sensitivity for many applications, as the one reported hereafter to quantify sulfasalazine.

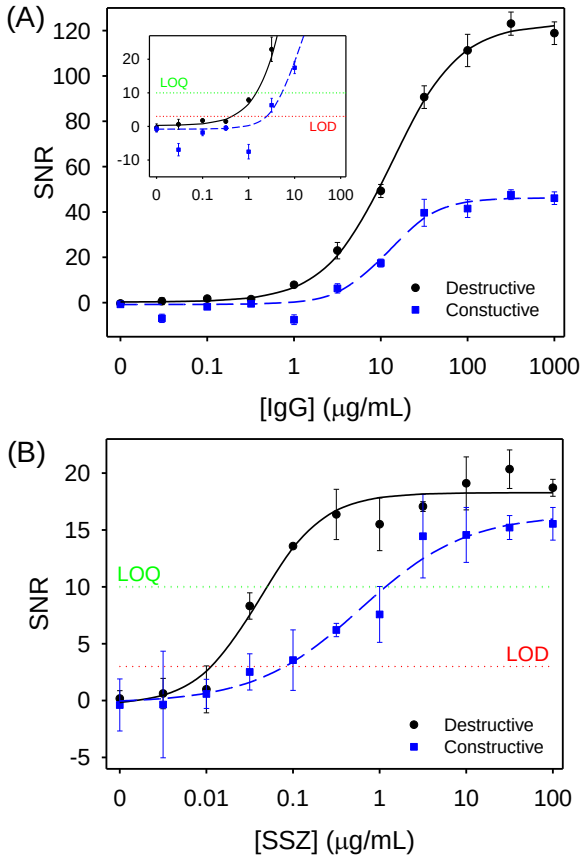

Fig. 4. Experimental dose-response curves for the destructive and constructive multilayered nanomaterials measured with the laser-scanning detection setup. (A) Results for the BSA/anti-BSA immunoassay. Data fitted to a four-parameter logistic equation ($R^2_{destruc.}$= 0.998 and $R^2_{construc.}$ = 0.983). Inset plot zooms in the detection and quantification limits. (B) Dose-response curves for competitive sulfasalazine immunoassay. Experimental data fitted to four-parameter logistic equation ($R^2_{destruc.}$= 0.974 and $R^2_{construc.}$ = 0.979). (A and B) Bottom and top dotted lines

mark the SNR thresholds for the detection and quantification limits (respectively) for both the constructive and destructive curves. Averaged values and standard deviations were calculated from 3 replicates.

Table 1. Features of exemplary developments in the scientific literature that address the determination of unlabeled antibodies and other proteins by optical biosensing.

Transduction principle	Probe	Target	LOD	LOD	reference
Guided-mode resonance	BSA	IgG	0.1 nM	16 ng mL^{-1}	[30]
Diffraction-based sensing	IgG	IgE	1.1 nM	200 ng mL^{-1}	[31]
Focal molography	IgG	IgG	1.3 nM	200 ng mL^{-1}	[32]
LSPR	IgG	IgG	12.5 nM	1880 ng mL^{-1}	[33]
Diffractive reflectance	biotin	streptavidin	25 nM	1375 ng mL^{-1}	[34]
SPR	IgG	HSA	1.5 nM	100 ng mL^{-1}	[35]
Interferometry	BSA	IgG	3.1 nM	460 ng mL^{-1}	This work

For the scope of this demonstration, we investigated the application of this interferometric approach for immunosensing low-molecular weight organic compounds. In particular, we focused on the label-free quantification of sulfasalazine, a sulfonamide (398,4 g/mol) commonly used as an anti-inflamatory drug [36]. This assay relies on the competition of the immobilized haptens (sulfasalazine analogues, S8) and the free analytes for the binding sites of the IgGs. Thus, although sulfasalazine molecules are too small to generate measurable changes in the biolayer thickness, their concentration can be determined by means of the IgGs bound to the hapten after the competition.

For this assay, microarrays of protein-hapten (OVA-S8) conjugates are immobilized on the surface of both nanomaterials and mixtures of sulfasalazine (different concentrations) and IgGs (constant concentration) are incubated on them. As observed in Fig. 4B, both dose-response curves showed the expected sigmoidal response. The constructive nanomaterial presented detection and quantification limits of 81 and 1170 ng mL^{-1} of unlabeled sulfasalazine, respectively. Whereas the destructive one displayed a more sensitive curve and reached detection and quantification limits of 11 and 50 ng mL^{-1}, respectively. To the best of our knowledge, other optical biosensing studies that quantify sulfasalazine in label-free conditions are not reported in the scientific literature. Therefore, we compared these results with the ones of other recent optical label-free

developments to sense other low-molecular weight organic compounds. As shown in Table 2, the detection limits herein reported are in the range of those in these representative examples of the state-of-the-art. Besides, the quantification limit herein obtained is lower than the 3 μg mL^{-1} of sulfasalazine present in serum samples after the recommended treatment dose of 2 g per day [37].

Besides, the interferometric behavior of these materials could also be potentially exploited to improve the reliability in bioanalysis. Most physical artifact sources in optical biosensing (dust, precipitates, substrate damage, etc.) absorb or scatter the incident light, thus generating unwanted signal decreases that interfere with the bioanalytical measurement. According to the design of these nanostructures, light intensities lower than the one of raw constructive substrates cannot be originated by the biointeraction and must come from experimental artifacts. Analogously, unwanted physical contributions that increased the intensity measured in raw destructive materials could also be identified as artifacts. Therefore, combining both nanomaterials for the same analysis is an appealing strategy to identify false positives and false negatives.

Table 2. Features of exemplary developments in the state-of-the-art that address the quantification of low-molecular weight organic compounds by optical label-free bioanalytical approaches.

Transduction principle	*Probe*	*Target*	*LOD (nM)*	*LOD (ng mL^{-1})*	*reference*
LSPR	*BSA-cortisol/IgG* [a]	*cortisol*	*22*	*8*	[38]
SPR	*BSA-imidacloprid/IgG* [a]	*imidacloprid*	*~ 4* [b]	*~ 1* [b]	[39]
Diffraction-based sensing	*BSA-2a/IgG* [a]	*atrazine*	*5.1*	*1.1*	[40]
BLI	*Saxitoxin/Aptamer*	*saxitoxin*	*1.7*	*0.5*	[41]
LSPR	*Au nanostars and MIPs*	*TNT*	*720*	*164*	[42]
Interferometry	*OVA-S8/IgG* [a]	*sulfasalazine*	*28*	*11*	*This work*

[a] Protein-hapten conjugates used together with selective IgGs in competitive assays.
[b] Visual detection limit.

3.4 One-shot interferometric biosensing

In addition to the sequential irradiation laser-scanning strategy described above, the bioanalytical system herein reported is also compatible with imaging approaches to scan the interferometric response of the whole microarray in one single shot. This section aims

to provide preliminary experimental insights into two different one-shot approaches that demonstrate further potential perspectives of this nanomaterials and introduce prospective routes for future advances. The first one also uses perpendicular irradiation with standard DVD laser units, but now the diameter of the incident beam must be expanded and the photodiode replaced by a camera, to capture the interferometric profile within the whole diameter of the beam. Preliminary results have been obtained in this direction (Fig. S6), which suggests prospective simplified laser-based scanning systems.

The other one-shot approach explored in this work consists of a color-based RGB interferometric measurement system. The interferences at around 650 nm generated by the biorecognition assays modify the overall polychromatic response and leads to color changes in the microarray spots. For the developed destructive materials, the color shifts from purple to blue for positive assays, and from goldish to reddish in the constructive ones (Fig. 3 top). Herein we propose a simple setup to quantify these events, which relies on a white light diffuse irradiation and a camera to capture color images of the microimmunoassays on the multilayered nanomaterials (Fig. S1B). With this configuration, the camera scans an area of about 15 x 15 millimeters.

As shown in Fig. 5A, the microarray observed in the captured RGB image is only comprised in the red channel, whereas the green and blue channels do not contain any analytical information. Also, the red channel is the only one that presents the expected destructive cross-section profile along the microarrayed immunoassay (Fig. 5B), and a signal proportional to the IgG concentration was also displayed by this approach (Fig. 5C). Although the correlation is lower than the previous one with the sequential irradiation setup, these preliminary results demonstrate that these interferometric nanomaterials are also compatible with one-shot approaches, which improves the scanning time of any detection system based on sequential irradiation and introduces promising alternatives for label-free biosensing.

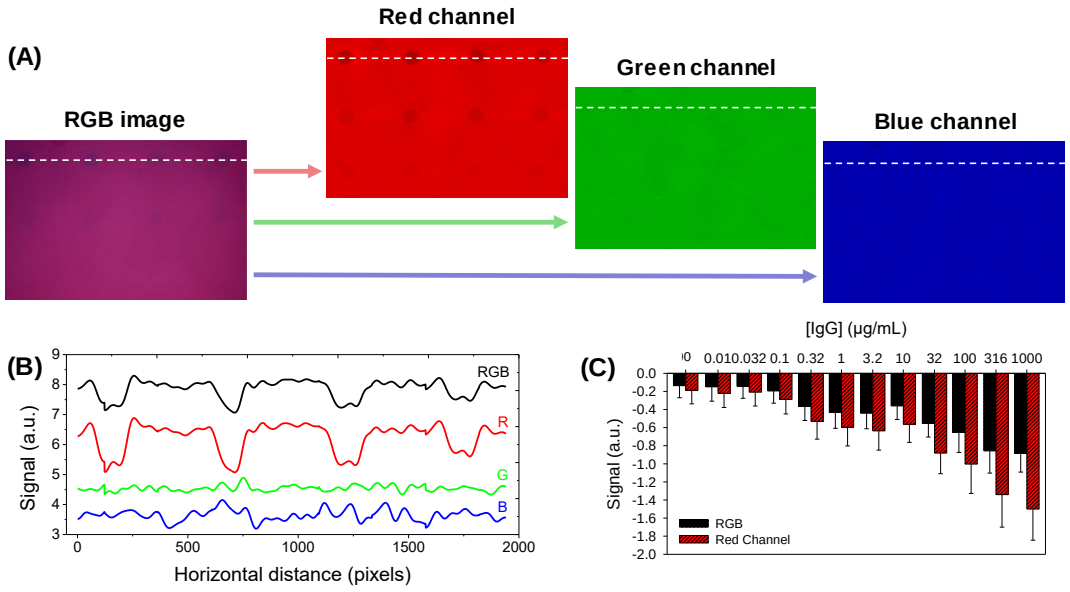

Fig. 5. Results of the color-based one-shot imaging system. (A) RGB image of a microarrayed BSA/anti-BSA immunoassay on a destructive multilayer, and its corresponding red, green, and blue channels. (B) Intensity cross-section profiles of the dashed white lines in the images above. A vertical offset was introduced in the curves to avoid overlapping and to simplify their visualization. (C) Dose-response curve of the immunoassay quantified from both the RGB image and the red channel (R^2_{RGB} = 0.939 and R^2_{Red} = 0.965, four-parameter logistic fitting).

4. Conclusions

This investigation demonstrates that the developed multilayered nanomaterials, constituted by superposed nanometric films of Ag-In-Sb-Te, ZnS, and Au on polycarbonate, allow label-free immunoassays to be quantified by interferometric imaging using simple reflection-based optical setups. By modifying the thicknesses profile of the multilayered structures, they can be tuned to transduce biorecognition events as both destructive and constructive interferences. The experimental results obtained in a model immunoassay and in a competitive immunoassay for low molecular weight organic compounds, demonstrate the bioanalytical performance of the approach and opens the door for its implementation in further applications and biorecognition assays. Although the destructive configuration presents a higher sensitivity, combining both structures introduces interesting options to improve the reliability in bioanalysis. In addition, the developed DVD laser-scanning system is a compact and inexpensive device with which the interferometric response of microarrayed assays on the nanomaterials can be successfully quantified by imaging. Furthermore, this detection system together with the structural and compositional features shared by these

multilayers and standard optical data-storage media, suggest prospective lab-on-a-disk advances. All this, along with the color-based one-shot approaches explored in this work, provide appealing insights to support the application and dissemination of optical nanomaterials for label-free biosensing out of specialized environments.

ASSOCIATED CONTENT

Supplementary Material

NOTES

The authors declare no competing financial interest.

ACKNOWLEDGMENT

This research was supported by FEDER and the Spanish Ministry of Economy and Competitiveness (CTQ2013-45875-R and CTQ2016-75749-R). The authors thank Ángel López Muñoz for the construction of the automatized positioning stage.

References:

[1] N. Khansili, G. Rattu, P.M. Krishna, Label-free optical biosensors for food and biological sensor applications, Sensors Actuators B Chem. 265 (2018) 35–49. https://doi.org/https://doi.org/10.1016/j.snb.2018.03.004.

[2] N.T. Darwish, S.D. Sekaran, S.M. Khor, Point-of-care tests: A review of advances in the emerging diagnostic tools for dengue virus infection, Sensors Actuators B Chem. 255 (2018) 3316–3331. https://doi.org/https://doi.org/10.1016/j.snb.2017.09.159.

[3] M.F.M. Fathil, M.K. Md Arshad, S.C.B. Gopinath, U. Hashim, R. Adzhri, R.M. Ayub, A.R. Ruslinda, M. Nuzaihan M.N., A.H. Azman, M. Zaki, T.-H. Tang, Diagnostics on acute myocardial infarction: Cardiac troponin biomarkers, Biosens. Bioelectron. 70 (2015) 209–220. https://doi.org/https://doi.org/10.1016/j.bios.2015.03.037.

[4] H. Kettler, K. White, S. Hawkes, Mapping the landscape of diagnostics for sexually transmitted infections: Key findings and recommandations, Unicef/Undp/World Bank/Who. (2004) 1–44.

[5] C. Chen, J. Wang, Optical biosensors: an exhaustive and comprehensive

review, Analyst. 145 (2020) 1605–1628. https://doi.org/10.1039/C9AN01998G.

[6] A. Kussrow, C.S. Enders, D.J. Bornhop, Interferometric methods for label-free molecular interaction studies, Anal. Chem. 84 (2012) 779–792. https://doi.org/10.1021/ac202812h.

[7] Q. Liu, Y. Shin, J.S. Kee, K.W. Kim, S.R. Mohamed Rafei, A.P. Perera, X. Tu, G.-Q. Lo, E. Ricci, M. Colombel, E. Chiong, J.P. Thiery, M.K. Park, Mach–Zehnder interferometer (MZI) point-of-care system for rapid multiplexed detection of microRNAs in human urine specimens, Biosens. Bioelectron. 71 (2015) 365–372. https://doi.org/10.1016/j.bios.2015.04.052.

[8] H.K.P. Mulder, C. Blum, V. Subramaniam, J.S. Kanger, Size-selective analyte detection with a Young interferometer sensor using multiple wavelengths, Opt. Express. 24 (2016) 8594. https://doi.org/10.1364/OE.24.008594.

[9] J. Escorihuela, M.Á. González-Martínez, J.L. López-Paz, R. Puchades, Á. Maquieira, D. Gimenez-Romero, Dual-polarization interferometry: a novel technique to light up the nanomolecular world, Chem. Rev. 115 (2015) 265–294. https://doi.org/10.1021/cr5002063.

[10] P. Kozma, F. Kehl, E. Ehrentreich-Förster, C. Stamm, F.F. Bier, Integrated planar optical waveguide interferometer biosensors: A comparative review, Biosens. Bioelectron. 58 (2014) 287–307. https://doi.org/10.1016/j.bios.2014.02.049.

[11] C.R. Mace, C.C. Striemer, B.L. Miller, Detection of human proteins using arrayed imaging reflectometry, Biosens. Bioelectron. 24 (2008) 334–337. https://doi.org/https://doi.org/10.1016/j.bios.2008.05.003.

[12] S. Rau, G. Gauglitz, Reflectometric interference spectroscopy (RIfS) as a new tool to measure in the complex matrix milk at low analyte concentration, Anal. Bioanal. Chem. 402 (2012) 529–536. https://doi.org/10.1007/s00216-011-5470-9.

[13] O. Avci, L.N. Ünlü, Y.A. Özkumur, S.M. Ünlü, Interferometric Reflectance Imaging Sensor (IRIS)—A Platform Technology for Multiplexed Diagnostics and Digital Detection, Sensors. 15 (2015) 17649–17665. https://doi.org/10.3390/s150717649.

[14] S.C.B. Gopinath, K. Awazu, P. Fons, J. Tominaga, P.K.R. Kumar, A sensitive multilayered structure suitable for biosensing on the BioDVD platform, Anal. Chem. 81 (2009) 4963–4970. https://doi.org/10.1021/ac802757z.

[15] S.C.B. Gopinath, K. Awazu, J. Tominaga, P.K.R. Kumar, Monitoring biomolecular interactions on a digital versatile disk: A BioDVD platform technology, ACS Nano. 2 (2008) 1885–1895. https://doi.org/10.1021/nn800285p.

[16] N. Pastor-Navarro, E. Gallego-Iglesias, Á. Maquieira, R. Puchades, Immunochemical method for sulfasalazine determination in human plasma, Anal. Chim. Acta. 583 (2007) 377–383. https://doi.org/10.1016/j.aca.2006.10.028.

[17] M. Avella-Oliver, J. Carrascosa, R. Puchades, Á. Maquieira, Diffractive Protein Gratings as Optically Active Transducers for High-Throughput Label-free Immunosensing, Anal. Chem. 89 (2017) 9002–9008. https://doi.org/10.1021/acs.analchem.7b01649.

[18] D. Necas, P. Klapetek, Gwyddion: an open-source software for SPM data analysis, Cent. Eur. J. Phys. 10 (2012) 181–188. https://doi.org/10.2478/s11534-

011-0096-2.

[19] M. Avella-Oliver, S. Morais, J. Carrascosa, R. Puchades, Á. Maquieira, Total analysis systems with thermochromic etching discs technology, Anal. Chem. 86 (2014) 12037–12046. https://doi.org/10.1021/ac502640j.

[20] M. Ozboyaci, D.B. Kokh, R.C. Wade, Three steps to gold: mechanism of protein adsorption revealed by Brownian and molecular dynamics simulations, Phys. Chem. Chem. Phys. 18 (2016) 10191–10200. https://doi.org/10.1039/C6CP00201C.

[21] H. Tashiro, M. Harigaya, Y. Kageyama, K. Ito, M. Shinotsuka, K. Tani, A. Watada, N. Yiwata, Y. Nakata, S. Emura, Structural analysis of Ag–In–Sb–Te phase-change material, Jpn. J. Appl. Phys. 41 (2002) 3758–3759. https://doi.org/10.1143/JJAP.41.3758.

[22] A. V Kolobov, P. Fons, A.I. Frenkel, A.L. Ankudinov, J. Tominaga, T. Uruga, Understanding the phase-change mechanism of rewritable optical media, Nat. Mater. 3 (2004) 703–708. https://doi.org/10.1038/nmat1215.

[23] G. Sancho-Fornes, M. Avella-Oliver, J. Carrascosa, S. Morais, R. Puchades, Á. Maquieira, Enhancing the sensitivity in optical biosensing by striped arrays and frequency-domain analysis, Sensors Actuators, B Chem. 281 (2019) 432–438. https://doi.org/10.1016/j.snb.2018.10.130.

[24] M. Avella-Oliver, R. Puchades, S. Wachsmann-Hogiu, A. Maquieira, Label-free SERS analysis of proteins and exosomes with large-scale substrates from recordable compact disks, Sensors Actuators, B Chem. 252 (2017) 657–662. https://doi.org/10.1016/j.snb.2017.06.058.

[25] G.A. López-Muñoz, M.-C. Estevez, E.C. Peláez-Gutierrez, A. Homs-Corbera, M.C. García-Hernandez, J.I. Imbaud, L.M. Lechuga, A label-free nanostructured plasmonic biosensor based on Blu-ray discs with integrated microfluidics for sensitive biodetection, Biosens. Bioelectron. 96 (2017) 260–267. https://doi.org/10.1016/J.BIOS.2017.05.020.

[26] M.C. Troparevsky, A.S. Sabau, A.R. Lupini, Z. Zhang, Transfer-matrix formalism for the calculation of optical response in multilayer systems: from coherent to incoherent interference., Opt. Express. 18 (2010) 24715–24721. https://doi.org/10.1364/OE.18.024715.

[27] X.B. Yin, B. Qi, X. Sun, X. Yang, E. Wang, 4-(Dimethylamino)butyric acid labeling for electrochemiluminescence detection of biological substances by increasing sensitivity with gold nanoparticle amplification, Anal. Chem. 77 (2005) 3525–3530. https://doi.org/10.1021/ac0503198.

[28] J.M. Martin, B. Trink, D. Daneman, H.-M. Dosch, B. Robinson, Milk Proteins in the Etiology of Insulin-Dependent Diabetes Mellitus (IDDM), Ann. Med. 23 (1991) 447–452. https://doi.org/10.3109/07853899109148088.

[29] S. Scarano, C. Scuffi, M. Mascini, M. Minunni, Surface Plasmon Resonance imaging-based sensing for anti-bovine immunoglobulins detection in human milk and serum, Anal. Chim. Acta. 707 (2011) 178–183. https://doi.org/https://doi.org/10.1016/j.aca.2011.09.012.

[30] G. Sancho-Fornes, M. Avella-Oliver, J. Carrascosa, E. Fernandez, E.M. Brun, Á. Maquieira, Disk-based one-dimensional photonic crystal slabs for label-free immunosensing, Biosens. Bioelectron. 126 (2019) 315–323. https://doi.org/10.1016/j.bios.2018.11.005.

[31] A. Juste-Dolz, M. Avella-Oliver, R. Puchades, A. Maquieira, Indirect microcontact printing to create functional patterns of physisorbed antibodies, Sensors (Switzerland). 18 (2018). https://doi.org/10.3390/s18093163.

[32] V. Gatterdam, A. Frutiger, K.-P. Stengele, D. Heindl, T. Lübbers, J. Vörös, C. Fattinger, Focal molography is a new method for the in situ analysis of molecular interactions in biological samples, Nat. Nanotechnol. 12 (2017) 1089–1095. https://doi.org/10.1038/nnano.2017.168.

[33] D. Hao, C. Hu, J. Grant, A. Glidle, D.R.S. Cumming, Hybrid localized surface plasmon resonance and quartz crystal microbalance sensor for label free biosensing, Biosens. Bioelectron. 100 (2018) 23–27. https://doi.org/https://doi.org/10.1016/j.bios.2017.08.038.

[34] W.-T. Chen, S.-S. Li, J.P. Chu, K.C. Feng, J.-K. Chen, Fabrication of ordered metallic glass nanotube arrays for label-free biosensing with diffractive reflectance, Biosens. Bioelectron. 102 (2018) 129–135. https://doi.org/https://doi.org/10.1016/j.bios.2017.10.023.

[35] E. Makhneva, Z. Farka, M. Pastucha, A. Obrusník, V. Horáčková, P. Skládal, L. Zajíčková, Maleic anhydride and acetylene plasma copolymer surfaces for SPR immunosensing, Anal. Bioanal. Chem. 411 (2019) 7689–7697. https://doi.org/10.1007/s00216-019-01979-9.

[36] J.K. Amaral, R. Sutaria, R.T. Schoen, Treatment of chronic chikungunya arthritis with methotrexate: a systematic review, Arthritis Care Res. (Hoboken). 70 (2018) 1501–1508. https://doi.org/10.1002/acr.23519.

[37] B. Nigović, S. Jurić, I. Mitrović, Bismuth nanoparticles-carbon nanotubes modified sensor for sulfasalazine analysis, Talanta. 164 (2017) 201–208. https://doi.org/10.1016/J.TALANTA.2016.11.059.

[38] J. Jeon, S. Uthaman, J. Lee, H. Hwang, G. Kim, P.J. Yoo, B.D. Hammock, C.S. Kim, Y.-S. Park, I.-K. Park, In-direct localized surface plasmon resonance (LSPR)-based nanosensors for highly sensitive and rapid detection of cortisol, Sensors Actuators B Chem. 266 (2018) 710–716. https://doi.org/https://doi.org/10.1016/j.snb.2018.03.167.

[39] K.-L. Lee, M.-L. You, C.-H. Tsai, E.-H. Lin, S.-Y. Hsieh, M.-H. Ho, J.-C. Hsu, P.-K. Wei, Nanoplasmonic biochips for rapid label-free detection of imidacloprid pesticides with a smartphone, Biosens. Bioelectron. 75 (2016) 88–95. https://doi.org/https://doi.org/10.1016/j.bios.2015.08.010.

[40] M. Avella-Oliver, V. Ferrando, J.A. Monsoriu, R. Puchades, A. Maquieira, A label-free diffraction-based sensing displacement immunosensor to quantify low molecular weight organic compounds, Anal. Chim. Acta. 1033 (2018) 173–179. https://doi.org/10.1016/j.aca.2018.05.060.

[41] S. Gao, X. Zheng, J. Wu, A biolayer interferometry-based competitive biosensor for rapid and sensitive detection of saxitoxin, Sensors Actuators B Chem. 246 (2017) 169–174. https://doi.org/https://doi.org/10.1016/j.snb.2017.02.078.

[42] N. Cennamo, A. Donà, P. Pallavicini, G. D'Agostino, G. Dacarro, L. Zeni, M. Pesavento, Sensitive detection of 2,4,6-trinitrotoluene by tridimensional monitoring of molecularly imprinted polymer with optical fiber and five-branched gold nanostars, Sensors Actuators B Chem. 208 (2015) 291–298. https://doi.org/https://doi.org/10.1016/j.snb.2014.10.079.